CONF-880613--24

DE89 003367

PRECIPITATION SENSITIVITY TO ALLOY COMPOSITION IN Fe-Cr-Mn AUSTENITIC STEELS DEVELOPED FOR REDUCED ACTIVATION FOR FUSION APPLICATION

P.J. Maziasz and R.L. Klueh

Metals and Ceramics Division, Oak Ridge
National Laboratory, Oak Ridge, TN 37831

ABSTRACT: Special austenitic steels are being designed in which alloying elements like Mo, Nb, and Ni are replaced with Mn, W, V, Ti, and/or Ta to reduce the long-term radioactivity induced by fusion reactor irradiation. However, the new steels still need to have properties otherwise similar to commercial steels like type 316. Precipitation strongly affects strength and radiation-resistance in austenitic steels during irradiation at 400-600°C, and precipitation is also usually quite sensitive to alloy composition. The initial stage of development was to define a base Fe-Cr-Mn-C composition that formed stable austenite after annealing and cold-working, and resisted recovery or excessive formation of coarse carbide and intermetallic phases during elevated temperature annealing. These studies produced a Fe-12Cr-20Mn-0.25C base alloy. The next stage was to add the minor alloying elements W, Ti, V, P, and B for more strength and radiation-resistance. One of the goals was to produce fine MC precipitation behavior similar to the Ti-modified Fe-Cr-Ni prime candidate alloy (PCA). Additions of Ti+V+P+B produced fine MC precipitation along network dislocations and recovery/recrystallization resistance in 20% cold worked material aged at 800°C for 166h, whereas W, Ti, W+Ti, or Ti+P+B additions did not. Addition of W+Ti+V+P+B also produced fine MC, but caused some σ phase formation and more recrystallization as well. These new alloys, therefore, achieved several of the initial design goals. Their fine MC precipitation and recovery/recrystallization behavior during aging is similar to that of the PCA. Calculations show that the new steels have over 10^3 times less long-term radioactivity than type 316.

KEY WORDS: austenitic steel, reduced activation, precipitation, MC, σ, χ, $M_{23}C_6$, recovery, recrystallization, radiation-resistance, alloy design, fusion

*Research sponsored by the Office of Fusion Energy, U.S. Department of Energy, under Contract No. DE-AC05-84OR21400 with the Martin Marietta Energy Systems, Inc.

INTRODUCTION

Austenitic Fe-Cr-Ni stainless steels are attractive as candidates for first-wall and structural materials for magnetic fusion reactor (MFR) applications, particularly near-term devices like the International Thermonuclear Experimental Reactor (ITER). Steels such as AISI 316 have good fabricability, strength, and ductility together with a large properties data base derived from commercial experience. Special Ti-modified austenitic stainless steels, like the prime candidate alloy (PCA) for the U.S. Fusion Materials Program, are the end product of years of alloy development efforts for radiation-resistance (resistance to void swelling and/or helium embrittlement) [1]. However, since the U.S. Department of Energy sponsored the Panel on Low Activation Materials in 1983 [2], awareness of the need to address the induced radioactivity issue for MFR structural components has increased.

Calculated radioactivity decay curves for various pure elements after exposure to a MFR neutron spectrum are shown in Fig. 1 [3]. This radioactive decay behavior defines several catagories for classifying potential MFR structural materials. The term *low-activation* ideally describes materials that would allow hands-on maintainence, and only materials like pure V or SiC can be classed as such. The term *fast induced-radioactivity decay* (FIRD) best describes engineering materials such as steels that would not allow hands-on maintainence, but could be disposed of by shallow land burial after reactor decommissioning [4]. A general strategy for the development of FIRD austenitic stainless steels was laid out by Klueh and Bloom in 1984 [4]. Replacement of elements like Mo, Nb, and Ni in Fe-Cr-Ni-Mo steels such as type 316 or the Ti-modified prime candidate alloy (PCA) with elements like Mn, W, Ti, V, Ta, Si and C would produce an acceptable FIRD alloy. Efforts by others in this direction have included investigating the irradiation behavior of either commercially available manganese stabilized steels (ie. AISI 200 series steels or

those produced by ARMCO or CREUSOT-MARREL) [5,6] or a wide range of pure or solute modified Fe-Cr-Mn alloys [7]. By contrast, the approach of the Fusion Materials Program at the Oak Ridge National Laboratory (ORNL) has been to attempt to produce a new FIRD manganese stabilized steel with properties equivalent to the PCA [4].

The ORNL program for developing manganese stabilized FIRD steels has been divided into several stages. The first stage involved selection of an appropriate Fe-Cr-Mn-C base alloy composition that would produce stable austenite in the range of 10-20 wt.% Cr, 13-19 % Mn and 0.07-0.4 % C [8-10]. From these alloys, a base composition of Fe-12Cr-20Mn-0.25C was selected for further alloying with minor element additions for more strength and radiation resistance [10]. The new phase information also led to the development of a modified Schaeffler diagram (originally developed for Fe-Cr-Ni alloys) for predicting the constituent phases of Fe-Cr-Mn-C alloys after annealing [11]. The second stage involved additions of appropriate amounts and combinations of W, Ti, V, P and B to produce fine, stable MC precipitation without upsetting the austenite stability of the base alloy or degrading its properties. Unirradiated mechanical properties and reactor irradiation response of the second stage alloys are currently being investigated. A third stage of alloy development will broaden the compositional range of the base alloy (ie., more Cr if more corrosion resistance is needed), adjust the minor element additions, and extend the scope of properties investigations, particularly if there is interest in these alloys for ITER.

The purpose of this paper is to examine the precipitation behavior and microstructural evolution of stage I and stage II alloys during high temperature aging in the cold worked condition. Data from stage I alloys was used in designing the stage II compositions. While thermal aging does not directly simulate irradiation

exposure, the behavior of radiation-resistant steels during reactor irradiation, particularly in high He/dpa ratio irradiation enviornments, has some relationship to their behavior during thermal aging at higher temperatures [2,12,13]. In austenitic stainless steels, recrystallization resistance of a heavily (20-25%) cold worked dislocation structure during high temperature aging is related to *(i)* the stability of the dislocations against recovery, *(ii)* the formation and stability characteristics of fine precipitates like MC that nucleate along dislocations and *(iii)* the resistance of the alloy to the formation of coarse carbide and intermetallic phases [2]. Radiation-resistant austenitic steels, like 25% CW PCA, experience enhanced-thermal microstructural evolution during reactor exposure because irradiation-induced processes (which cause unusual and often undesirable microstructural evolution that is usually very different from thermal aging) are suppressed [2,12-14]. MC precipitate formation and stability is crucial for causing the point defect mechanisms which produce void swelling resistance to operate, particularly at the higher He/dpa ratios expected in an MFR first-wall [12,13,15]. This approach of controlling precipitation behavior was first used to design new PCA (14Cr-16Ni) steels modified with minor solutes. These new Fe-Cr-Ni steels are more void swelling resistant during HFIR irradiation at 500°C than the origninal PCA, due to better MC formation and stability [16]. Improved MC behavior also gives these same steels outstanding thermal creep resistance at 700°C [17]. The focus, therefore, during stage II of the FIRD alloy development effort was what influence minor element additions have on MC formation and recrystallization of these new Fe-Cr-Mn alloys during aging at 800°C.

EXPERIMENTAL

In stage I, fifteen 500g heats of Fe-Mn-Cr-C alloys (PCMA-0 thru -14) were cast at ORNL to determine a stable austenitic base composition, and then seven more alloys (PCMA-15 thru -21), with various combinations of minor alloying element additions made to a Fe-20Mn-12Cr-0.25C base composition, were cast in Stage II. The compositions of these various alloys are given in Tables 1 and 2. More details on production and fabrication of these alloys can be found elsewhere [8,9,11].

The PCMA-0 through -9 alloys were annealed for 1h at 1150°C after casting and then cold rolled to a 30% reduction in area. Samples were then either aged for 166h at 800°C or homogenized for 24h at 1275°C and reannealed for 1h at 1150°C or 8h at 1050°C. The PCMA-10 through -21 alloys were hot rolled at 1050°C to a 50% reduction in area and then homogenized for 5h at 1200°C. Final 0.76mm sheet was produced by several cold rolling steps of up to 50% with intermediate anneals of 1h at 1150°C; the final sheet was in the 20% cold-worked (CW) condition. Samples of this material were then either aged for 168h at 800°C or reannealed for 1-2h at 1150°C or 8h at 1050°C.

Most of the specimens were examined using metallography or analytical electron microscopy techniques and for magnetic phase content using a FERRITE-SCOPE to detect magnetic eddy currents. Transmission electron microscopy (TEM) was performed using JEM 100C, 100CX, and 2000FX and PHILIPS EM430 and CM-12 instruments; matrix and precipitate phases were identified by using selected-area and convergent-beam electron diffraction techniques (SAD and CBED, respectively) as well as X-ray energy dispersive spectroscopy (XEDS) for quantitative compositional

analysis (JEM 2000FX with TN 5500 Series II Analyzer or PHILIPS EM400T/FEG with EDAX 9100 Analyzer).

RESULTS

Phase Formation in Annealed Stage I Alloys

After annealing for 1-2h at 1150°C, most of the stage I alloys contained other phases in addition to the austenite matrix except for PCMA-7 and PCMA-12 alloys, which were completely austenitic. The phases identified in each alloy after annealing are listed in Table 3. Metallography of the microstructure of PCMA-7 is shown in Fig. 2c and TEM of PCMA-12 is shown in Fig. 3. Alloys PMCA-0 through -2 contained large amounts of δ-ferrite due to their low C and high Cr contents (Table 1) and were highly magnetic [8]. A typical microstructure for this group of alloys is shown for PCMA-2 in Fig. 2a. The PCMA-4 alloy with low Cr and high Mn contents had a significant amount of martensite in the as-annealed microstructure. This phase appeared to be ϵ-martensite (hexagonal close packed, HCP) because this sample was not highly magnetic [8]. After 30% cold working, however, PCMA-4 became very magnetic, presumable due to the formation of strain-induced α'-martensite (body centered tetragonal, BCT) [18]. The PCMA-10 through -14 alloys, all with about 20 wt.% Mn, tend to confirm these effects of alloy composition on ϵ-martensite and δ-ferrite formation. Alloys 10 and 11 with lower Cr contents form ϵ-martensite, while alloys 13 and 14 with more Cr form δ-ferrite. In general, the alloys with about 20 wt.% Mn had more austenite and less of the other phases than alloys with less Mn.

The PCMA-5 through -9 alloys generally had higher C and Cr contents and formed primarily austenite with similar amounts of δ-ferrite at grain boundary triple point junctions and varying amounts of carbide phase (presumably $M_{23}C_6$) within the δ-ferrite particles. The microstructures of PCMA-6, -7 and -9 are shown in Fig. 2. PCMA-7 with the most C and Cr (0.36 and 19 wt.%, respectively) was completely austenitic. PMCA-6 contained γ + δ phases with only a few carbides whereas PCMA-9 contained copious carbide precipitation within the δ-ferrite phase (see Figs. 2b and 2d). These results, together with the behavior of the PCMA-10 through -14 alloys show the need to balance Mn, Cr and C additions to produce a stable austenitic alloy. The Mn and C contents must both be raised to keep the austenite free of martensite, but above about 15-16 wt.% Cr, it is difficult to keep the microstructure free of δ-ferrite and carbides. The TEM microstructure and AEM composition of a δ-ferrite particle analyzed in annealed PCMA-14 is shown in Fig. 4 (also see Table 4). The δ-ferrite phase has more Cr than the γ-austenite matrix. Since Cr-rich carbides form within the δ-ferrite particles in PCMAs -6 and -9, C appears to be less soluble in the δ-ferrite than in the austenite.

Phase Formation in Cold-Worked and Aged Stage I Alloys

Metallographic and TEM investigations of PCMA-0 through -9 alloys that had been 30% cold worked and those aged for 168h at 800°C showed varying amounts of recovery and/or recrystallization together with the precipitation of carbide and/or intermetallic (σ) phases (see Table 3 for phases). There was no evidence ferrite or martensite in the aged materials and little or no detectable ferromagnetic behavior. Only the PCMA-1 alloy with the lowest C content (0.01 wt.%) showed any detectable ferromagnetism. This could indicate a small amount of δ-ferrite present

with the abundance of σ-phase particles found in this sample. Metallography of PMCA-2, -6, -7, and -9 after aging is shown in Fig. 5 (compare with annealed alloys in Fig. 2). The PCMA-1, -2 and -4 alloys recrystallized completely into a new assembly of small grains (see PCMA-2 in Fig. 5a), whereas the PCMA-5 through -9 alloys retained the austenite grain structure established by annealing prior to cold working (Figs. 5b and 5d). During aging, the entirely austenitic PCMA-7 was more recovery/recrystallization resistant than the other alloys (Fig. 5c).

The TEM examination showed that recrystallization of the PCMA-1 through -4 alloys produced dislocation-free grains with a high density of extended stacking faults. Examples of this type of microstructure are shown in Fig. 6a and 6b for alloys PCMA-2 and -4, respectively. The PCMA-5 through -9 alloys had either higher uniform dislocation contents or non-uniform mixtures of regions with higher dislocation network concentrations and dislocation-free regions. Both PMCA-7 and -9 had finer structures of stacking faults and a uniformly higher density of network dislocations, as shown in Figs. 6c and 6d.

TEM observations also revealed considerable precipitation of coarse σ and $M_{23}C_6$ (τ) phases after aging (see Table 3). The PCMA-1 alloy (lowest C) formed mainly σ phase, whereas the PCMA-7 alloy (highest C) contained mainly $M_{23}C_6$ phase. The other alloys had mixtures of coarse (0.5 - 5 μm in diam.) σ and $M_{23}C_6$ phases in the γ matrix, with PCMA-2 and -9 appearing to have the most abundant precipitation [18]. Figure 7 shows a typical σ-phase particle with a low order CBED zone-axis pattern (ZAP) that clearly identifies the phase. Only the PCMA-7 alloy that resisted recovery/recrystallization contained a uniform dispersion of fine $M_{23}C_6$ particles, as shown in Fig. 8, along with a (001) CBED-ZAP.

The compositions of several coarse σ and $M_{23}C_6$ particles in PCMA-9 were determined via quantitative XEDS in-foil analyses, and data are given in Table 4.

The $M_{23}C_6$ phase was mainly Cr-rich, whereas the σ-phase was rich in Fe and Cr. The phase compositions in this Fe-Cr-Mn-C steel were generally similar to those observed for the same phases formed in aged type 316 stainless steel (Fe-Cr-Ni-Mo) [14], but these phases found in the Mn-stabilized steels contain significant amounts of Mn (see Table 4), while both phases formed in aged type 316 are low in Mn and Ni.

The PCMA-10 through -14 alloys were also aged for 166h at 800°C in the 20% cold worked condition, but were only examined by metallography and with regard to magnetic behavior. No ferromagnetic phases were detectable after aging, although small amounts of either α'-martensite or δ-ferrite were detected in the cold worked material prior to aging [9].

Phase Formation in Annealed Stage II Alloys

As a result of the Phase I studies, base composition of Fe-12Cr-20Mn-0.25C (MnCrC or PCMA-15) was selected for the stage II alloys, and minor element solute additions were made to this base composition to improve its strength [10,11]. The nomenclature chosen to designate the alloys indicates the solute additions made to the base composition (ie. Ti addition is designated MnCrCTi). The stage II alloys were cold worked 20% and then annealed for 2h at 1150°C. All of the alloys were fully austenitic after annealing, but contained varying small amounts of $M_{23}C_6$ and/or MC carbides. The phases found in these alloys are listed in Table 3 and metallography of six of the seven alloys is shown in Fig. 9.

The base MnCrC alloy contained a sparce dispersion of inclusions after annealing and little or no precipitation was detected metallographically. The MnCrCTi, MnCrCW, and MnCrCTiW alloys had similar grain sizes and microstructures

after annealing, but contained different amounts of precipitation. The MnCrCW alloy had little or no precipitation (see Fig. 9b), while the other two alloys had uniform dispersions of fine (on a lower magnification, metallographic scale) precipitates throughout the grains (Figs 9a and 9c); there was no obvious precipitation along grain boundaries. By contrast, the MnCrCTiBP, MnCrCTiVBP, and MnCrCTiVWBP alloys showed distinct precipitation along grain boundaries, as shown in Figs. 9d - 9f. The MnCrCTiVBP and MnCrCTiVWBP alloys also showed somewhat more intragranular precipitation than the MnCrCTiBP alloy.

TEM analysis showed that most of the alloys had some coarse or fine precipitates along the grain boundaries after annealing, (Fig. 10); diffraction analysis was used to identify the phases (Table 3). All of the alloys contained some MC and/or $M_{23}C_6$ carbides along grain boundaries or within the grains, consistent with the metallographic data in Fig. 9. However, additional details were revealed by the higher magnification TEM examination that were not obvious in Fig. 9. The MnCrC base alloy had very fine $M_{23}C_6$ particles distributed along the grain boundaries (Fig. 10a), but no precipitation was detected within the grains. The MnCrCTi alloy had fine intergranular MC together with some coarse particles in the matrix (Fig. 10b). The MnCrCW alloy had coarse $M_{23}C_6$ along the grain boundaries (Fig. 10c), whereas MnCrCTiW steel had a mixture of coarse $M_{23}C_6$ and MC intragranularly, but virtually no precipitation along the boundaries (Fig. 10d). The MnCrCTiBP, MnCrCTiVBP, and MnCrCTiWVBP alloys all contain similar distributions of coarse, blocky carbides along the grain boundaries (Figs. 10e and 10f) and some within the grains. The alloys with Ti+B+P and Ti+V+B+P had only MC phase particles, whereas the Ti+V+W+B+P alloy formed a mixture of MC and $M_{23}C_6$.

The morphological character of the high-angle, incoherent grain boundaries changed significantly with minor alloying element composition. After annealing,

nearly all of the grain boundaries in the alloys without B and P (PCMA-15 through -18) were quite straight, similar to the boundary shown for PCMA-12 in Fig. 3. However, the grain boundaries in the alloys which contained trace additions of B and P (PCMA-19 through -21), had a zig-zag or kinked shape, with kink nodes occuring at the precipitate particles (Figs. 10e and 10f).

Phase Formation in Cold-Worked and Aged Stage II Alloys

The stage II alloys were cold worked 20% and then aged for 168h at 800°C. Specimens were examined using TEM and AEM and diffraction and characteristic XEDS techniques were used for phase identification. Lower magnification TEM showed recovery/recrystallization behavior in several alloys (Fig. 11). The base MnCrC alloy showed some recrystallization after aging, and recovery occurred in the regions that did not completely recrystallize (Fig. 11a). Aging also produced coarse $M_{23}C_6$ particles (Table 3 and Table 4).

In comparison to the base alloy, the alloys with solute additions of Ti, W, and Ti+W were more prone to recovery and/or recrystallization. The representative microstructure of the MnCrCTi alloy is shown in Fig. 11b to be almost fully recrystallized, with only small, isolated patches of deformed material remaining. The other two alloys showed more recovery but less large, dislocation-free grains. All of these alloys had significant amounts of coarse precipitation primarily in the recrystallized regions. The MnCrCTi and MnCrCTiW alloys, both of which contained Ti, had mixtures of coarse $M_{23}C_6$ and MC particles, while the MnCrCW alloy formed coarse $M_{23}C_6$ and particles of another phase that were rich in Cr and Fe, but did not appear to be either σ or χ phases (Tables 3 and 4).

By contrast, the alloys modified with the solutes Ti+B+P, Ti+V+B+P, and Ti+W+V+B+P were quite resistant to recrystallization and recovery. The MnCrCTiV-BP alloy showed the least recrystallization (Fig. 11c), while MnCrCTiBP had the least amount of coarse precipitation; most of the coarse phase particles in these two alloys were $M_{23}C_6$ (Table 4). The MnCrCTiWVBP alloy had somewhat more recrystallization than the other two alloys in this last group, but it also had the most coarse precipitation. These coarse particles in MnCrCTiWVBP were a mixture of $M_{23}C_6$ and σ phases, and the recrystallized regions were either associated with very coarse precipitates in the matrix or heavily precipitated grain boundaries, or both (Fig. 11d).

Higher magnification TEM provided a closer look at recovery of the dislocation structure and revealed fine precipitation in the unrecrystallized regions in these aged alloys, as shown in Fig. 12. Fine precipitation was not detected in the base MnCrC alloy or in the alloy with only W added (Fig. 12b). Only sparce amounts of very fine (2-6nm in diam.) precipitation were detected in the alloys modified with only Ti or with Ti+B+P (Figs. 12a and 12d). The particles were too small and too few for sufficient electron diffraction, but their presence in the alloys with Ti additions suggests that they could be MC phase. In the MnCrCTi alloy, there were only a few recovered regions, whereas in the MnCrCW and MnCrCTiBP alloys which were much more resistant to recovery/recrystallization (particularly the latter), there were higher concentrations of large, intersecting faults. Both of these latter alloys also appeared to have many dislocations which had dissociated into partials so that fault fringes were visible. Both features can be seen in Figs. 12b and 12d, but they are especially prominent in Fig. 12b for PCMA-17. Although detailed Burgers vector analysis was not performed, these differences were quite noticable when comparing one alloy with another. Widely separated partial dislocations would

suggest that some of the alloying additions had lowered the stacking fault energy relative to the base alloy.

The PCMA-18, -20 and -21 alloys all had abundant dispersions of fine MC distributed throughout the unrecrystallized matrix regions, as shown in Figs. 12c, 12e and 12f, respectively. The MC phase was easily identified by diffraction analysis with its characteristic cube-on-cube crystallographic habit relative to the γ-austenite matrix. The alloys modified with Ti+V+B+P and Ti+W+V+B+P showed more resistance to recovery than the alloy with only Ti+P, which despite only a modest amount of recrystallization did show large recovered regions, with loose tangles of dislocation network and a coarser structure of the intragranular faulted-bands common to many of these steels (ie. Figs. 11c and 11d). Figure 12c shows that many of the fine MC particles in the MnCrCTiW steel are not directly associated with the visible network dislocations, whereas there is a high degree of association between dislocation segments and fine MC particles in the MnCrCTiVBP and MnCrCTiWVBP steels shown in Figs. 12e and 12f, respectively. Many of the dislocations also showed fault contrast images in the alloys modified with Ti+V+B+P and Ti+W+V+B+P, suggestive of dissociation and lower stacking fault energy, whereas the dislocations in the Ti+W alloy did not. These observations suggest that the MC-dislocation association and the splitting of dislocations into partials are in fact related. Dissociated dislocations would be less mobile and more easily pinned by fine precipitate particles. These detailed observations are indeed consistent with the good recovery/recrystallization resistance exhibited by the MnCrCTiVBP and MnCrCTiWVBP alloys during aging at temperatures as high as 800°C.

Calculations of Radiocative Decay Behavior with Time for the Stage II Alloys

An important goal in the development of FIRD alloys is that they show less long-term residual radioactivity than conventional steels such as type 316 stainless steel, and that they meet the 10 CFR 61 Class C requirements for waste disposal by shallow land burial [4]. The radioactive decay behavior as a function of time after exposure to MFR irradiation for a typical heat of type 316 and for the actual composition of one of the solute-modified Fe-12Cr-20Mn steels (PCMA-21, Table 2) were calculated by F. M. Mann [19] of the Westinghouse Hanford Company (Fig. 13). While normal chemical analysis showed less than 0.01 wt.% Nb in the MnCrCTiWVBP (PCMA-21) steel, the normal detectability limit for such techniques, residual element analysis using spark-source mass spectrometry, was not performed on these Mn-stabilized steels, and they were assumed to have 0.0001 wt.% Nb. Normal chemistry methods show that some heats of type 316 have up to about 0.1 wt.% Nb [16], while trace element analysis methods show Nb levels in other heats as low as 0.0005 wt.% [20]. Niobium is not an intentional alloying addition to type 316. Figure 13 shows that long-term irradiation exposure (10y or 36 MWy/m^2) in a commercial conceptual MFR like STARFIRE produces roughly similar levels of radioactivity in type 316 and the new FIRD Fe-Cr-Mn steels immediately after shutdown. However, after a period of about 50-100y, the residual radioactivity of a FIRD alloy like PMCA-21 is over 10^3 times less than that found in conventional type 316. Comparison of several other classes of alloys together with type 316 and PCMA-21 steels is made in Fig. 14, by expressing the ratio of calculated radioactivity to that allowed by 10 CFR 61 Class C standard. Numbers greater than 1 indicate that the materials do not qualify as Class C waste, whereas numbers of 1 or less mean that they do qualify. None of the alloys qualify for class C disposal after irradiation to STAR-

FIRE-type conditions, although "low-activation" alloys come much closer than conventional materials like type 316 or 9Cr-1MoVNb steels. Similar calculations and comparisons for much lower irradiation exposures (1.4y or 5 MWy/m^2) in a STAR-FIRE-type machine indicate that FIRD steels like PCMA-21 can then qualify as Class C waste, whereas type 316 cannot.

DISCUSSION

The systematic alloy development approach pursued at ORNL for FIRD Fe-Cr-Mn steels has been successful in terms of the goals initially set [4,8]. The stage I alloys revealed Fe-Cr-Mn-C compositions in which austenite was stable, without δ-ferrite formation during high-temperature annealing, or ϵ- and α'- martensite formation after cooling to room temperature or cold working [10,11]. These same experimental data also produced enough new information to modify the normal Schaefler that describes Fe-Cr-Ni alloys to adequately describe Fe-Cr-Mn-C alloys as well [11]. The new diagram was used to define the base Fe-12Cr-20Mn-0.25C alloy composition for the stage II solute modified alloys. The microstructural results of the stage I alloys made it clear that with more than 15-16 wt.% Cr, it was difficult to keep the austenite free of δ-ferrite and carbides at most levels of Mn and C. At lower Cr contents, it was important to have at least enough C to prevent martensite from forming.

The results for cold worked stage I alloys aged at 800°C showed that the ϵ- and α'-martensite and δ-ferrite phases of concern in the annealed material are replaced by concerns about the formation of coarse σ and $M_{23}C_6$ phases during aging. One very important aging result from the PCMA-0 through -9 alloys was that the most stable austenitic alloy (PCMA-7) was the most resistant to the

formation of coarse $M_{23}C_6$ and σ phases during aging. Carbon has been found to be very important for resistance to intermetallic phase formation during the development of Fe-Cr-Ni steels optimized for irradiation resistance [2]. Consistently, the lack of C in pure Fe-Cr-Mn alloys studied by Garner and co-workers appears to be part of the reason for excessive formation of σ phase in those alloys during FBR irradiation or during high temperature aging [21-23]. The other important result from aging studies of the first alloy series was the formation of fine $M_{23}C_6$ precipitates in the alloy with the highest C content. These finely dispersed precipitates are obviously related to the recovery/recystallization resistance of that alloy (PCMA-7), which in turn may also relate to σ phase resistance. The formation of σ phase often occurs in conjunction with recrystallization in both the stage I and II alloys investigated in this work, and Garner et al. [22] recently presented more detailed data and mechanisms for σ phase formation in the recrystallized grains of Fe-Cr-Mn ternary alloys. The formation of fine $M_{23}C_6$ precipitation in PCMA-7 probably reflects the fact that as the kinetics of carbide precipitation increase with increasing C supersaturation, precipitation becomes rapid enough to occur before recrystallization. Precipitate nucleation along the dislocations in the cold-worked structure would naturally be much easier and finer than nucleation in the recrystallized grains.

The annealing studies of the stage II solute modified alloys produced several important results. Most of minor alloying elements added to the base alloy were ferritizing elements, but all of the alloys were still fully austenitic after annealing. The base alloy did not contain excessive carbide precipitation after annealing, which would indicate the solubility limit for carbon had not been exceeded. The effect of the minor solutes varied, but the alloys that had precipitation of carbides along the grain boundaries did not contain excessive carbide precipitation within the grains.

Commercial Fe-Cr-Mn steels considered in several other studies have C contents that range from 0.02 to 0.6 wt.%, and our alloys fall within that range. Most of the commercial alloys also contain N contents that range from 0.02 to 0.6% as well, and current FIRD guidelines limit N to much lower levels [24]. Some commercial high-Mn steels, like the Russian EP-838 steel, contain Ni and Al additions, and most contain up to 0.02 wt.% P, but none appear to contain the W, Ti, V, and B additions explored in the steels being developed at ORNL. The higher C content of the MnCrC and various solute modified steels required annealing at about 1150°C or more, because annealing at 1050°C generally produced more precipitation than 1150°C. The effect of the minor alloying elements on grain boundary morphology and precipitation behavior are probably important to the processing behavior, because the MnCrCTiBP and MnCrCTiWVBP alloys with zig-zag grain boundary shape and coarser MC + $M_{23}C_6$ precipitates did not exhibit excessive grain growth at 1150°C (Figs. 10e and 10f). These grain boundary precipitate effects could also be important for strength at temperatures of 600-800°C [2].

The recrystallization resistance of the PCMA-19 through -21 alloys and the fine, stable MC observed in the MnCrCTiVBP and MnCrCTiWVBP steels are important results from the studies of cold-worked and aged stage II alloys. While these initial solute-modified alloys are not yet optimized, their recrystallization resistance and fine MC microstructures are similar to the original PCA alloy and newer solute-modified versions of the PCA given the same cold-work + aging test [2,25]. This similarity was one of the goals set to measure alloy development progress for these alloys, particularly with regard to achieving radiation-resistance. Several recent studies of swelling resistance in the Fe-14Cr-16Ni PCA or JPCA (a closely related Japanese heat of Ti-modified steel) irradiated in HFIR have shown that the swelling resistance of these steels depends on the formation and stability of fine MC

precipitation during irradiation at high He generation rates [2,26,27]. Therefore, we believe that the MC-formation characteristics of the MnCrCTiVBP and MnCrCTiWV-BP alloys represent significant progress toward our goals for stage II of our alloy-development program. In recent work, a wide range of binary and ternary Fe-Cr-Mn alloys irradiated in FFTF at 400-600°C showed significant swelling. However, swelling was similar to or in some cases less than comparable Fe-Cr-Ni alloys [7,22]. Similar irradiation studies in FFTF show that cold work reduces swelling in the binary Fe-Mn and ternary Fe-Cr-Mn alloys, and that various commerial high-Mn steels can have better swelling resistance in the cold-worked condition after irradiation to about 80 dpa, particularly at 420°C [22,23]. Although these irradition results do not include the He/dpa generation ratio expected for an MFR first wall and include alloys that do not meet the FIRD compositional requirements, they nonetheless support our approach to alloy development. This approach includes producing alloys with stable dispersions of fine precipitates and stable cold-worked dislocation structures. The effects of minor solutes, either alone or synergistically with other elements, on subtle phenomena like stacking-fault energy, dislocation dissociation, and dislocation pinning by fine precipitates are preliminary results that will require careful study to confirm and understand. However, they are important to our expectations for the effectiveness of microstructural design and control for radiation-resistance.

All of the stage II alloys are currently being irradiated in experiments in the Fast Flux Test Facility - Materials Opened Test Assembly (FFTF-MOTA) to determine swelling resistance in solution-annealed and 20% cold worked material at 400-600°C (irradiations began with reactor cycle 9).

The calculations shown in Figs. 13 and 14 indicate the progress made in reducing long-term radioactivity in these Fe-Cr-Mn FIRD alloys, and the results of

Fig. 14b for lower dose irradiation provide encouragement for considering these steels in design studies of near-term fusion devices like ITER. New FIRD steels like the MnCrCTiWVBP steel can meet the 10 CFR-61 Class C requirements for shallow land burial after fusion irradiation, whereas commercial steels like type 316 cannot. We are therefore beginning stage III of our alloy development to look at more alloys over a wider range of Cr-Mn levels while continuing to study the effects of combinations of minor element solute additions and to expand the properties investigations to include corrosion, welding and other properties of interest.

Finally, it is worth mentioning that based on the effect that solute modifications have on producing fine precipitate dispersions and recovery/recrystallization resistance during aging at 800°C, the FIRD steels may also be useful for non-fusion applica-tions requiring high-temperature strength and/or creep resistance. The base alloy (PCMA-15) showed good work hardening characteristics relative to type 316 [10]. Recent efforts to produce tailored structures of fine precipitates for strength with similar solute modifications in Fe-14Cr-16Ni austenitic stainless steels [2] have resulted in steels with excellent creep-rupture resistance at 700°C (up to 10^3 times better than type 316) [28]. Since these new FIRD steels contain Mn instead of Ni and have lower contents of strategic materials like Cr and Mo, they are probably cheaper as well. Recently, Tamura et al. from Nippon-Kokan and the Japanese Atomic Energy Research Institute (JAERI) [29] have also developed a FIRD Fe-14Cr-25Mn-0.25C steel modified with 0.2 wt.% Ti. They find good weldability relative to JPCA and suggest that corrosion resistance in water should be better than Fe-Cr-Ni steels. Thus, these new FIRD steels, or similar steels with less rigid compositional restrictions, may also have non-fusion spin-off applications.

CONCLUSIONS

1. A series of Fe-Cr-Mn-C alloys, annealed for 1-2h at 1150°C, demonstrated that a stable austenitic steel could be produced with a composition of Fe-12Cr-20Mn with 0.2-0.25 wt.% C. Alloys with high Mn and low C contained ϵ-martensite after annealing and often formed α'-martensite during subsequent cold working. Alloys with >15% Cr and >0.2% C contained δ-ferrite.

2. The same series of Fe-Cr-Mn-C alloys cold worked and then aged for 168h at 800°C showed that alloys that were not entirely austenitic after annealing were also prone to excessive formation of coarse $M_{23}C_6$ and σ-phase particles and/or recrystallization and recovery. The austenitic PCMA-7 (Fe-15Cr-19Mn) with 0.4 wt.% was resistant to recrystallization and recovery, and contained finely dispersed $M_{23}C_6$ particles.

3. A series of alloys with minor additions of combinations of Ti, W, V, P and B were made to a base composition of Fe-12Cr-20Mn-0.25C. These alloys were entirely austenitic after annealing for 2h at 1150°C. Most contained either coarse or fine carbides ($M_{23}C_6$ and/or MC) along very straight grain boundaries or in the matrix. However, the alloys modified with additions of Ti+B+P, Ti+V+B+P, and Ti+W+V+B+P all had peculiar zig-zag shaped grain boundaries which contained carbides.

4. After cold working and then aging for 168h at 800°C, the alloys modified with solute additions of Ti+B+P, Ti+V+B+P, and Ti+W+V+B+P were the most resistant to recrystallization and recovery, with the Ti+V+B+P alloy being the best of this group.

Only the alloys modified with both Ti and W (PCMA-18, -20 and -21) had abundant disperions of fine MC precipitation along the dislocation network. The Ti+V+B+P alloy had the least amount of coarse $M_{23}C_6$, and only the alloy with all the solutes (PCMA-21) had some σ-phase.

5. The fine MC precipitate microstructures and recrystallization and recovery behavior at 800°C of PCMA-20 and -21 are similar to the behavior of the Ti-modified Fe-Cr-Ni PCA steel. These results represent significant progress toward one of the goals of the ORNL development program for Fe-Cr-Mn FIRD steels.

6. Calculations of the decay of fusion-induced radiocativity with time indicate about a 10^3 reduction 50-100y after shutdown for PCMA-21 relative to type 316, and the potential to meet Class C burial requirements.

REFERENCES

1. Conn, R.W., et al. "Panel Report on Low Activation Materials for Fusion Applications," UCLA Report PPG-728, University of California at Los Angeles, June 1983.

2. Maziasz, P.J., *MiCon 86: Optimization of Processing, Properties, and Service Performance through Microstructural Control*, ASTM STP 979, eds. B.L. Bramfitt, et al., Am. Soc. for Testing and Matls., Philadelphia, PA, 1988, p. 116.

3. Calculations by F.W. Mann, Westinghouse Hanford Company, Richland WA, 1982.

4. Klueh, R.L. and Bloom, E.E., *Alloy Development for Fast Induced Radioactivity*

Decay for Fusion Reactor Applications, ORNL/TM-8944, Oak Ridge National Laboratory Report, March 1984.

5. Fenici, P., et al., *Nucl. Engin. Des./Fusion* 1 (1984) 167.

6. Gelles, D.S. and Garner, F.A., *J. Nucl. Mater.* 133&134 (1985) 521.

7. Brager, H.R., et. al., *J. Nucl. Mater.* 133&134 (1985) 907.

8. Klueh, R.L. and Maziasz, P.J., *ADIP Semiannu. Prog. Rept., Sept. 30, 1984*, DOE/ER-0045/13, U.S.D.O.E., (March, 1985) p. 69.

9. Klueh, R.L. and Maziasz, P.J., *ADIP Semiannu. Prog. Rept., Sept. 30, 1985*, DOE/ER-0045/15, U.S.D.O.E. Office of Fusion Energy, (February, 1986) p. 69.

10. Klueh, R.L. and Maziasz, P.J., "Reduced-Activation Austenitic Stainless Steels: The Fe-Mn-Cr-C System," published elsewhere in these proceedings.

11. Klueh, R.L., Maziasz, P.J., and Lee, E.H., *Matls. Sci. and Engin.*, 102 (1988) 115.

12. Maziasz, P.J., *J. Nucl. Mater.* 122 & 123 (1984) 472.

13. Maziasz, P.J., *J. Nucl. Mater.* 108 & 109 (1982) 359.

14. Maziasz, P.J. and McHargue, C.J., *Internat. Matls. Rev.* 32 (1987) 190.

15. Stoller, R.E., et al., "Swelling Behavior of Austenitic Stainless Steels in a Spectrally Tailored Reactor Experiment: Implications for Near-Term Fusion Machines," to be published in *J. Nucl. Mater.* 1988.

16. Maziasz, P.J., et al., *Fusion Reactor Materials Semiannu. Prog. Rept., March 31, 1987*, DOE/ER-0313/2, U.S.D.O.E. Office of Fusion Energy, (Sept. 1987) p. 188.

17. Maziasz, P.J. and Swindeman, R.W., Proc. Internat. Conf. *Advances in Materials Technology for Fossil Power Plants*, A.S.M.-International, Metals Park, OH (1987) p. 283.

18. Maziasz, P.J. and Klueh, R.L., *ADIP Semiannu. Prog. Rept., Sept. 30, 1985*, DOE/ER-0045/15, U.S.D.O.E. Office of Fusion Energy, (February, 1986) p. 54.

19. Mann, F.M., *Fusion Reactor Materials Semiannu. Prog. Rept., March 31, 1988*, DOE/ER-0313/4, U.S.D.O.E. Office of Fusion Energy, (Aug. 1988) p. 12.

20. Maziasz, P.J., Conf. Proc. *Phase Stability During Irradiation*, eds. Holland, J.R., Mansur, L.K., and Potter, D.I., The Metallurgical Society of AIME, Warrendale, PA (1981) p. 477.

21. McCarthy, J.M. and Garner, F.A., *Fusion Reactor Materials Semiannu. Prog. Rept., Sept. 30, 1987*, DOE/ER-0313/3, U.S.D.O.E. Office of Fusion Energy, (Mar., 1988) p. 115.

22. Garner, F.A., Abe, F. and Noda, T., *Fusion Reactor Materials Semiannu. Prog. Rept., Sept. 30, 1987*, DOE/ER-0313/3, U.S.D.O.E. Office of Fusion Energy, (Mar., 1988) p. 123.

23. McCarthy, J.M. and Garner, F.A., *Fusion Reactor Materials Semiannu. Prog. Rept., March 31, 1988*, DOE/ER-0313/4, U.S.D.O.E. Office of Fusion Energy, (Aug. 1988) p. 146.

24. Doran, D.G., Rowcliffe, A.F. and Mann, F.M., *J. Nucl. Mater.*, 141-143 (1986) 1074.

25. Maziasz, P.J. and Jitsukawa, S., *ADIP Semiannu. Prog. Rept., March 31, 1985*, DOE/ER-0045/14, U.S.D.O.E. Office of Fusion Energy, (July, 1985) p. 37.

26. Tanaka, M.P. et al., *J. Nucl. Mater.*, 141-143 (1986) 943.

27. Tanaka, M.P. et al. "Microstructural Development of Austenitic Stainless Steels Irradiated in HFIR," to be published in *J. Nucl. Mater.* in 1988.

28. Maziasz, P.J. and Swindeman, R.W., Proc. Internat. Conf. *Advances in Materials Technology for Fossil Power Plants*, eds. Viswanathan, R. and Jaffee, R.I., ASM-International, Metals Park, OH (1987) p. 283.

29. Tamura, M., et al., *J. Nucl. Mater.*, 141-143 (1986) 1067.

FIGURE CAPTIONS

1. A plot of the calculated radioactivity (in Curies/cm^3) induced in various pure elements by irradiation in a MFR neutron spectrum and its decay as a function of time after reactor shutdown (taken from Wiffen and Santoro, Proc. of *Topical Conference on Ferritic Alloys for Use in Nuclear Energy Technologies*, TMS-AIME, 1984, p. 195).

2. Metallography showing the microstructure developed after annealing 30% cold worked material for 1h at 1150°C in alloys a.) PCMA-2, b.) PCMA-6, c.) PCMA-7, and d.) PCMA-9.

3. TEM of the fully austenitic microstructure developed in PCMA-12 after annealing 20% cold-worked material for 1h at 1150°C.

4. TEM of a δ-ferrite particle formed in PCMA-14 during annealing for 1h at 1150°C. The histogram shows the composition of the precipitate particle and the adjacent matrix as determined by quantitative XEDS analysis.

5. Metallography of the microstructures developed after aging 30% cold-worked material for 166h at 800°C in alloys a.) PCMA-2, b.) PCMA-6, c.) PCMA-7, and d.) PCMA-9.

6. TEM of the microstructures developed after aging 30% cold worked material for 166h at 800°C in alloys a.) PCMA-2, b.) PCMA-4, c.) PCMA-7, and d.) PCMA-9.

7. a.) TEM of a σ-phase particle formed in 30% cold worked PCMA-6 during aging for 166h at 800°C and b.) CBED of the (001)σ ZAP for identification.

8. TEM of fine $M_{23}C_6$ (τ) particles formed in 30% cold worked PCMA-7 during aging for 166h at 800°C, imaged in a.) bright-field and b.) dark-field using a τ reflection, with c.) CBED of the (001)τ ZAP for identification.

9. Metallography of the microstructures developed after annealing 20% cold worked material for 2h at 1150°C in alloys a.) MnCrCTi, b.) MnCrCW, c.) MnCrCTiW, d.) MnCrCTiBP, e.) MnCrCTiVBP, and f.) MnCrCTiWVBP.

10. TEM of the microstructures developed at the grain boundaries after annealing 20% cold-worked material for 2h at 1150°C in alloys a.) MnCrC, b.) MnCrCTi, c.) MnCrCW, d.) MnCrCTiW, e.) MnCrCTiBP, and f.) MnCrCTiWVBP.

11. Lower magnification TEM of the microstructures developed after aging 20% cold-worked material for 168h at 800°C in alloys a.) MnCrC, b.) MnCrCTi, c.) MnCrCTi-VBP, and d.) MnCrCTiWVBP.

12. TEM of the fine precipitate and dislocation microstructures developed in the matrix after aging 20% cold-worked material for 168h at 800°C in alloys a.) MnCrCTi, b.) MnCrCW, c.) MnCrCTiW, d.) MnCrCTiBP, e.) MnCrCTiVBP, and f.) MnCrCTiWVBP.

13. A plot of the calculated radioactivity (in Curies/cm^3) induced in type 316 stainless steel and in a new ORNL FIRD steel (PCMA-21) by irradiation in a MFR neutron spectrum and its decay as a function of time after reactor shutdown (courtesy of F.M. Mann, 1988 [19]).

14. Histograms of the ratio of calculated radioactivity decay behavior with time after shutdown to that allowed by the 10 CFR-61 Class C standard for various conventional and reduced activation first wall materials being considered by the U.S. Fusion Materials Program exposed to irradiation in a STARFIRE fusion reactor spectrum for a.) 10y or 36MWy/m^2 and b.) 1.4y or 5 MWy/m^2 (courtesy of F.M. Mann, 1988 [19]).

Table 1. Chemical Compositions of Phase I Alloys

Alloy Designation	Composition, wt %[a]			
	Mn	Cr	C	N
PCMA-0	13.4	15.0	0.07	0.001
PCMA-1	14.2	14.8	0.01	0.001
PCMA-2	17.1	15.2	0.056	0.001
PCMA-3	13.9	10.0	0.09	0.002
PCMA-4	18.9	9.9	0.093	0.002
PCMA-5	13.9	15.3	0.18	0.002
PCMA-6	14.3	16.0	0.18	0.003
PCMA-7	19.1	14.8	0.38	0.005
PCMA-8	17.7	20.1	0.13	0.003
PCMA-9	17.6	20.2	0.26	0.006
PCMA-10	19.9	10.0	0.081	0.005
PCMA-11	20.0	11.9	0.084	0.009
PCMA-12	20.0	11.95	0.18	0.008
PCMA-13	19.1	14.0	0.088	0.013
PCMA-14	19.9	15.9	0.17	0.0012

[a]Balance iron.

Table 2. Chemical Compositions of Phase II Alloys

Alloy Designation	Composition, wt %[a]						
	Mn	Cr	C	W	Ti	V	Other
MnCrC (PCMA-15)	20.6	11.8	0.24	<0.01	<0.01	0.01	
MnCrCTi (PCMA-16)	20.5	11.7	0.25	0.09	0.11	0.01	
MnCrCW (PCMA-17)	20.5	11.8	0.23	0.83	<0.01	0.01	
MnCrCTiW (PCMA-18	21.1	11.7	0.25	0.77	0.12	0.01	
MnCrCTiBP (PCMA-19)	20.5	11.9	0.24	<0.01	0.10	0.01	B, P
MnCrCTiVBP (PCMA-20)	20.8	11.8	0.22	<0.01	0.10	0.10	B, P
MnCrCTiWVBP (PCMA-21)	20.4	11.7	0.25	1.08	0.10	0.10	B, P

[a]Balance iron.

Table 3. Qualitative microstructural phase identification in annealed or cold-worked and aged Fe-Mn-Cr-C alloys

Alloy	Phases Identified	
	SA (1 to 2 h at 1150°C)	20 to 30% Cold-Worked and Aged (166 h at 800°C)
	Stage I Alloys[a]	
PCMA-0	γ + δ	n.d.
PCMA-1	γ + δ	γ + σ
PCMA-2	γ + δ	γ + σ + $M_{23}C_6$
PCMA-3	γ + δ	n.d.
PCMA-4	γ + M	γ + $M_{23}C_6$ + σ
PCMA-5	γ + δ + M	n.d.
PCMA-6	γ + δ + carbides	γ + σ + $M_{23}C_6$
PCMA-7	γ	γ + $M_{23}C_6$
PCMA-8	γ + δ + carbides	n.d.
PCMA-9	γ + δ + carbides	γ + $M_{23}C_6$ + σ
PCMA-10	γ + M	n.d.
PCMA-11	γ + M	n.d.
PCMA-12	γ	n.d.
PCMA-13	γ + δ	n.d.
PCMA-14	γ + δ	n.d.
	Stage II Alloys[b]	
MnCrC	$M_{23}C_6$	$M_{23}C_6$
MnCrCTi	MC	$M_{23}C_6$ + MC
MnCrCW	$M_{23}C_6$	$M_{23}C_6$ + some Fe and Cr-rich phases
MnCrCTiW	$M_{23}C_6$ + MC	$M_{23}C_6$ + MC
MnCrCTiBP	MC	$M_{23}C_6$ + MC
MnCrCTiVBP	MC	$M_{23}C_6$ + MC
MnCrCTiWVBP	$M_{23}C_6$ + MC	$M_{23}C_6$ + MC + σ

[a]Identified with either metallography or TEM/AEM techniques.

γ – austenite, δ – ferrite, M – martensite, σ – sigma phase.

[b]Identified with both metallography and TEM/AEM techniques.

Table 4. Quantitative XEDS compositional analyses of in-foil precipitate phase particles in Fe-Cr-Mn-C alloys

Phase	Composition,[a] at. %						
	Si	Ti	V	Cr	Mn	Fe	W
PCMA-14, SA 1 h at 1150°C							
δ-ferrite (3)[b]			0.2	23.1	19.6	56.7	
PCMA-9, 30% CW + Aged 168 h at 800°C							
τ-$M_{23}C_6$ (2)				73.0	12.0	14.9	
σ-phase (1)				28.8	18.7	51.2	
MnCrC, 20% CW + Aged 168 h at 800°C							
τ-$M_{23}C_6$ (6)	0.3	0.1	0.1	66.5	14.8	18.0	
MnCrCTi, 20% CW + Aged 168 h at 800°C							
τ-$M_{23}C_6$ (2)		0.1	0.1	67.4	14.6	17.5	0.3
MC (3)		77.6	0.2	3.6	4.9	9.5	4.2
MnCrCW, 20% CW + Aged 168 h at 800°C							
τ-$M_{23}C_6$ (3)		0.1	0.1	65.0	14.7	17.5	2.7
Fe-rich phase (2)		0.1	0.1	36.3	17.8	44.4	1.5
Cr-rich phase (2)		0.1	0.1	46.5	16.8	34.7	1.8
MnCrCTiW, 20% CW + Aged 168 h at 800°C							
τ-$M_{23}C_6$ (2)		0.1	0.3	67.5	13.4	16.2	2.1
MC (1)		67.4		3.3	5.1	13.1	11.0
MnCrCTiVBP, 20% CW + Aged 168 h at 800°C							
τ-$M_{23}C_6$ (2)		0.2	0.7	63.4	15.8	19.8	0
MnCrCTiBP, 20% CW + Aged 168 h at 800°C							
τ-$M_{23}C_6$ (2)		0.1		66.6	14.8	18.5	
MnCrCTiWVBP, 20% CW + Aged 168 h at 800°C							
τ-$M_{23}C_6$ (2)		0.2	0.8	63.9	14.0	17.9	3.0
σ-phase (2)			0.2	22.0	21.0	54.3	2.5

[a]Composition of metal atoms heavier than aluminum.

[b]Number of particles analyzed.

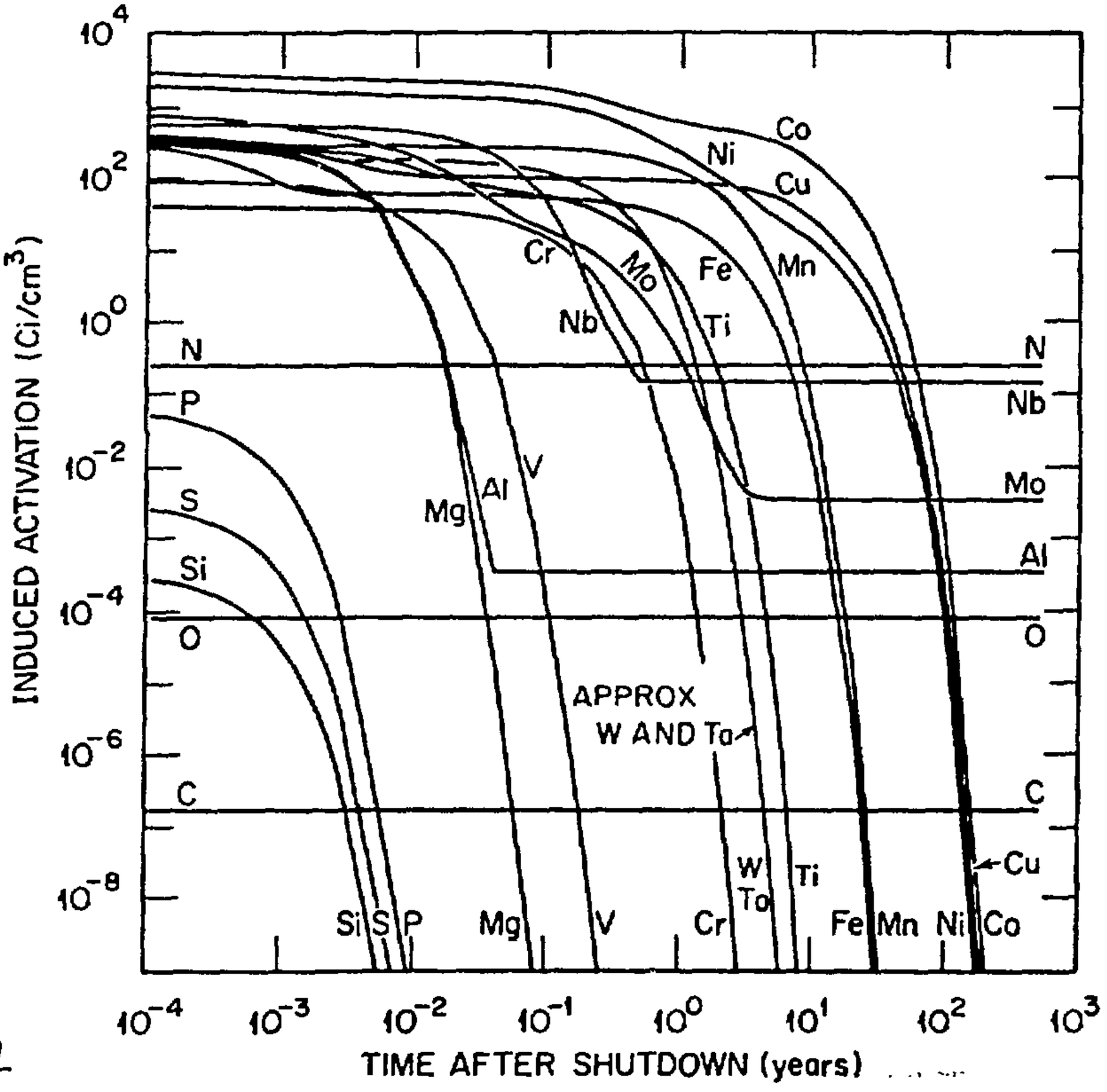
INDUCED ACTIVATION (Ci/cm³)
TIME AFTER SHUTDOWN (years)
Co
Ni
Cu
Cr
Mo
Fe
Mn
Nb
Ti
N
P
S
Si
Mg
Al
V
O
C
APPROX
W AND Ta
W
Ta
Ti
Cu
Si S P Mg V Cr Fe Mn Ni Co

Fig. 1

Fig. 2

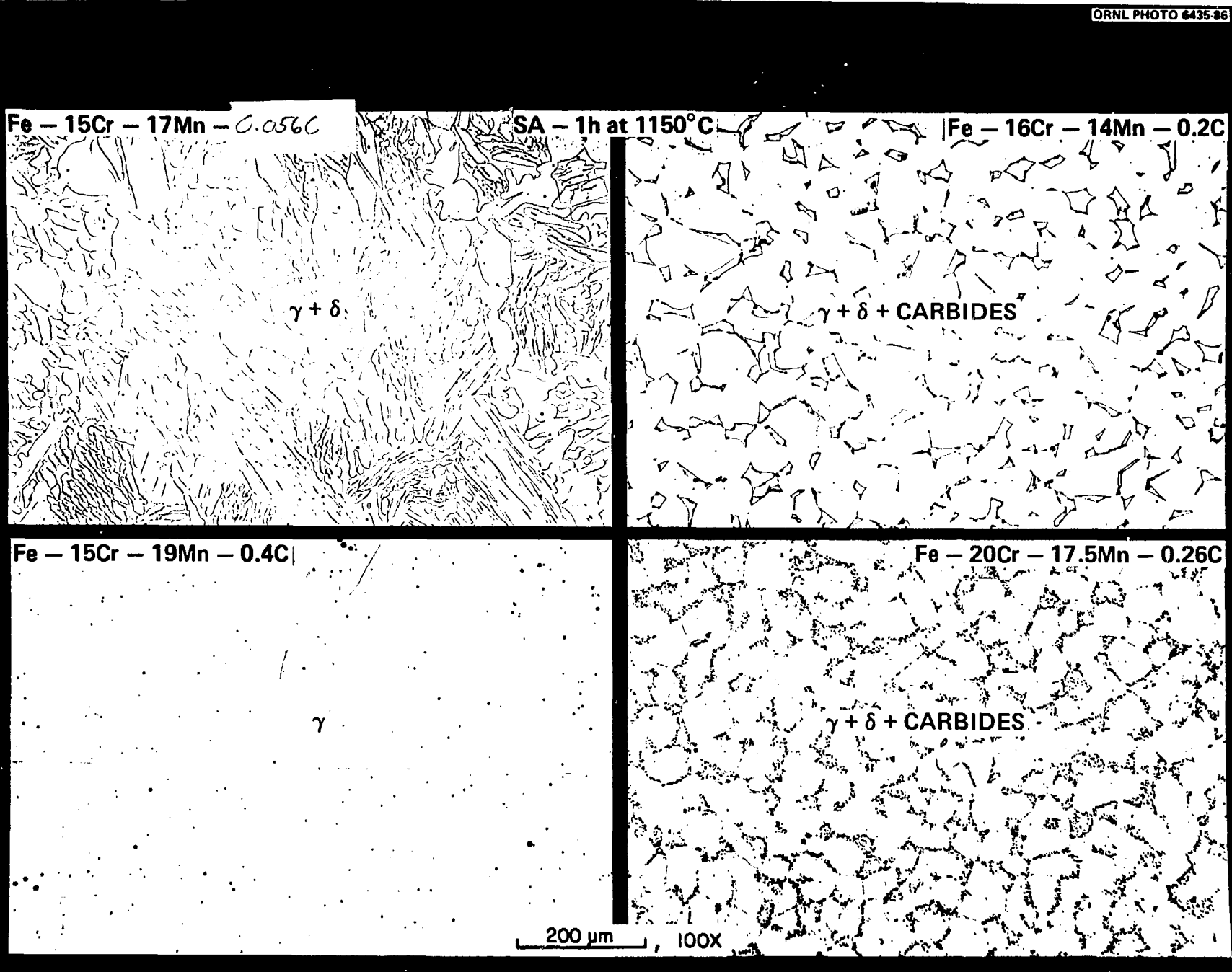
ORNL PHOTO 6435-86
Fe – 15Cr – 17Mn – 0.05C
SA – 1h at 1150°C
γ + δ
Fe – 16Cr – 14Mn – 0.2C
γ + δ + CARBIDES
Fe – 15Cr – 19Mn – 0.4C
γ
Fe – 20Cr – 17.5Mn – 0.26C
γ + δ + CARBIDES
200 μm
100X

E 49178 YE 13062

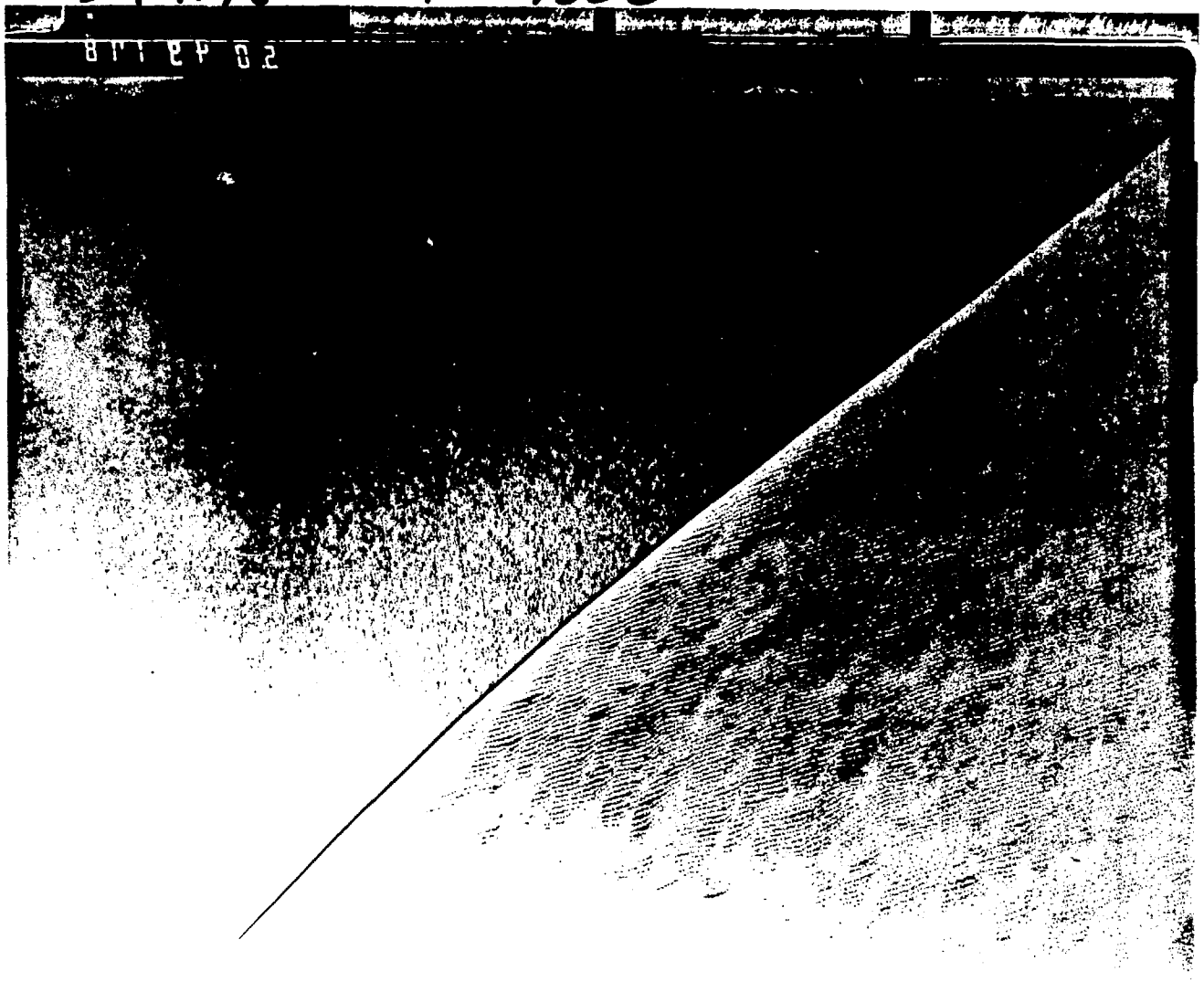

1 μm

Fig. 3

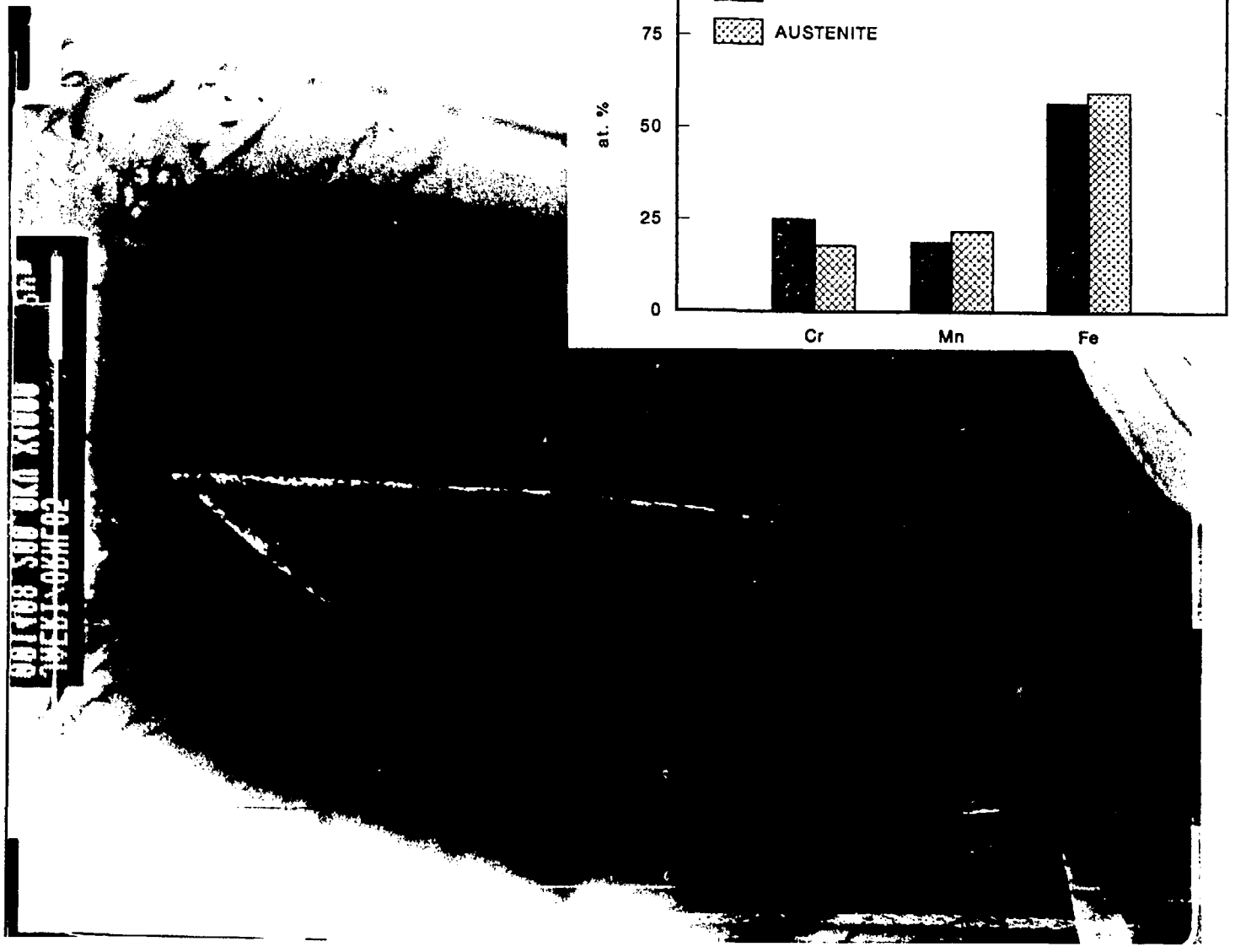

Fig. B4.

Fig. 5a 200 μm 100X

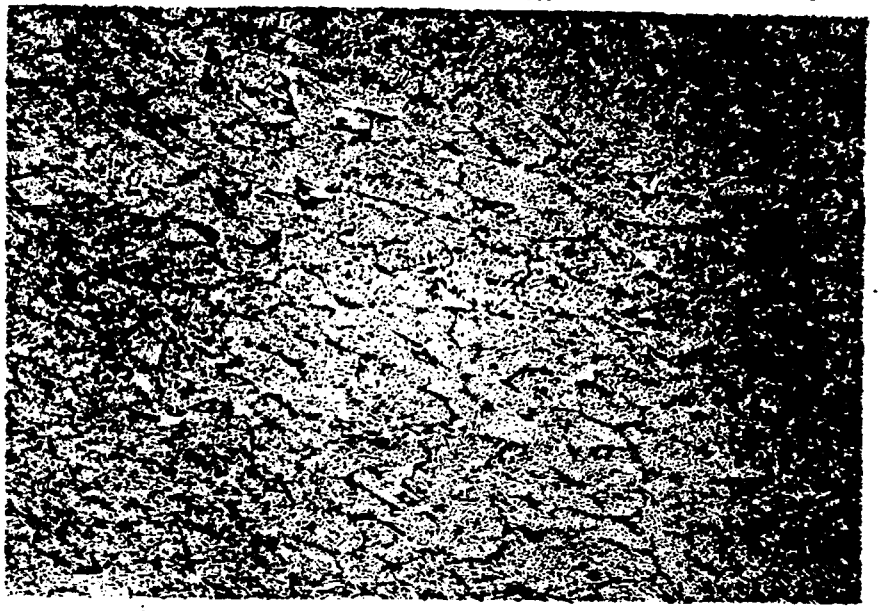

5b

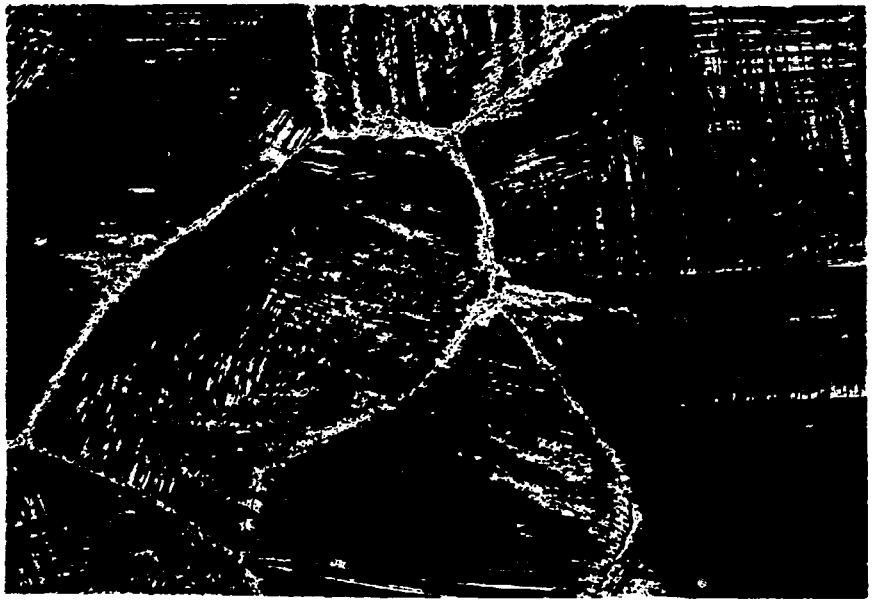

5c. 200 μm 100X

5d. 200 μm 100X

4E13064

Fig. 6a

1 μm

485621 4E13070

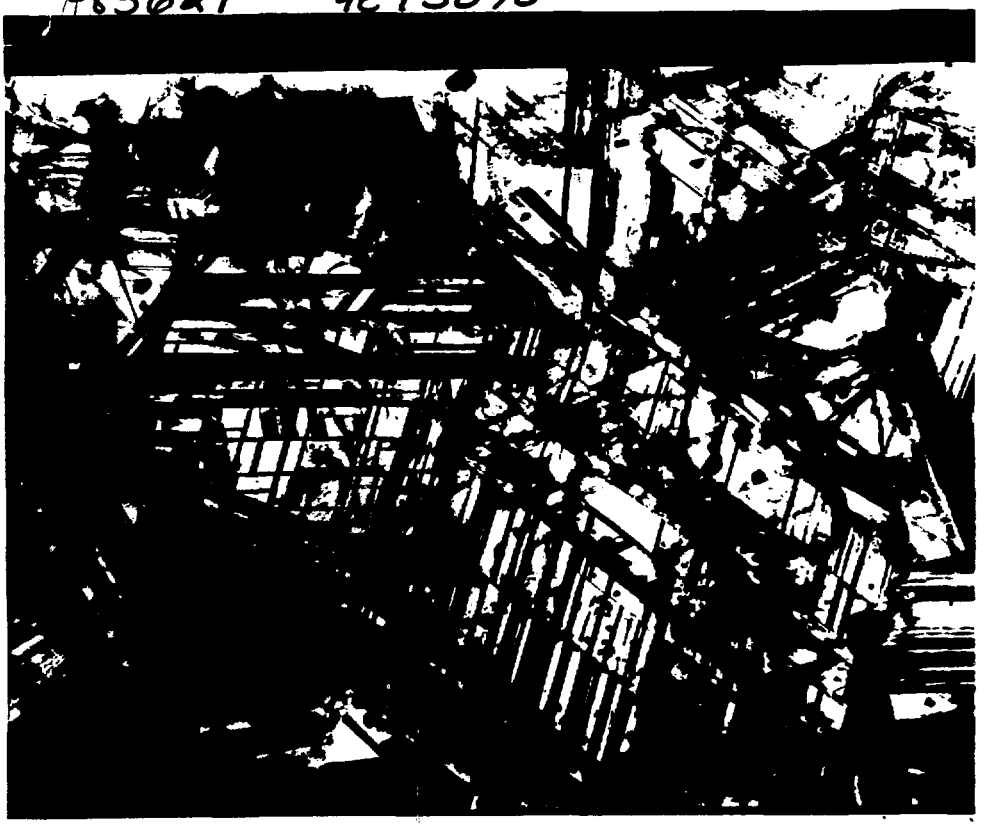

6b.

H85565 4E 13065

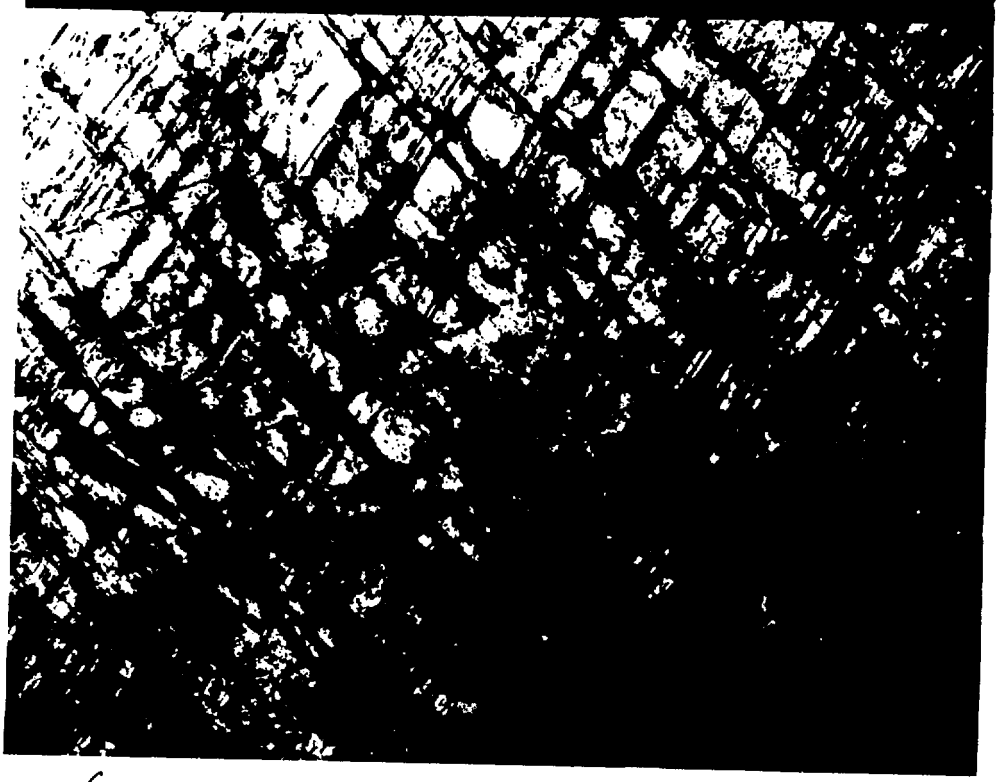

6c.

H85598 4E13066

6d.

Fig. 7a

482059 4E 13078 1 µm

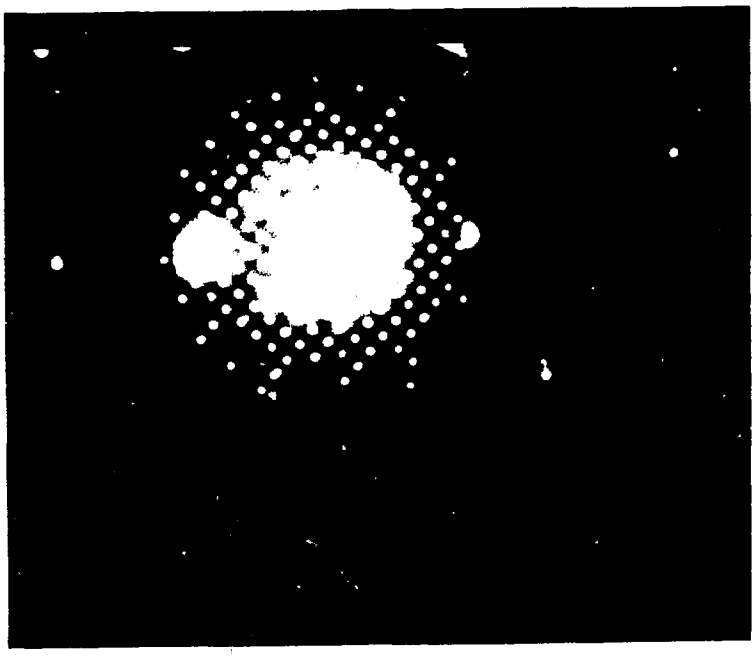

Fig. 7b

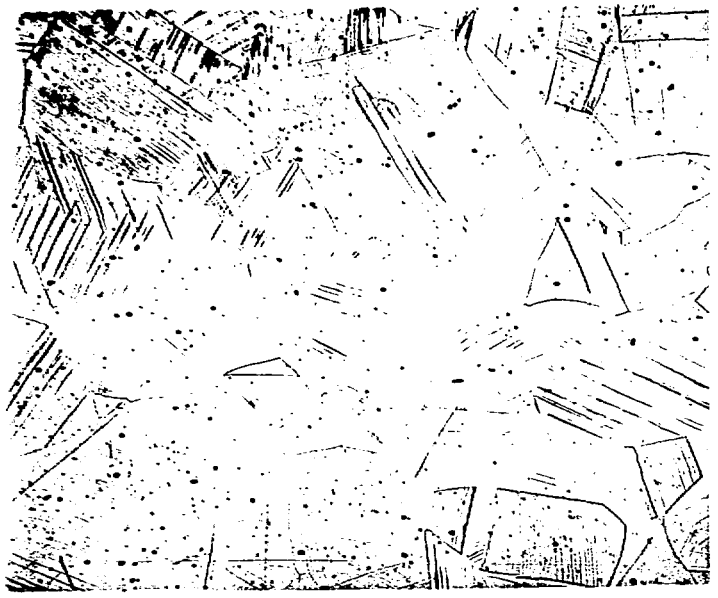

9b 100 µm 200X

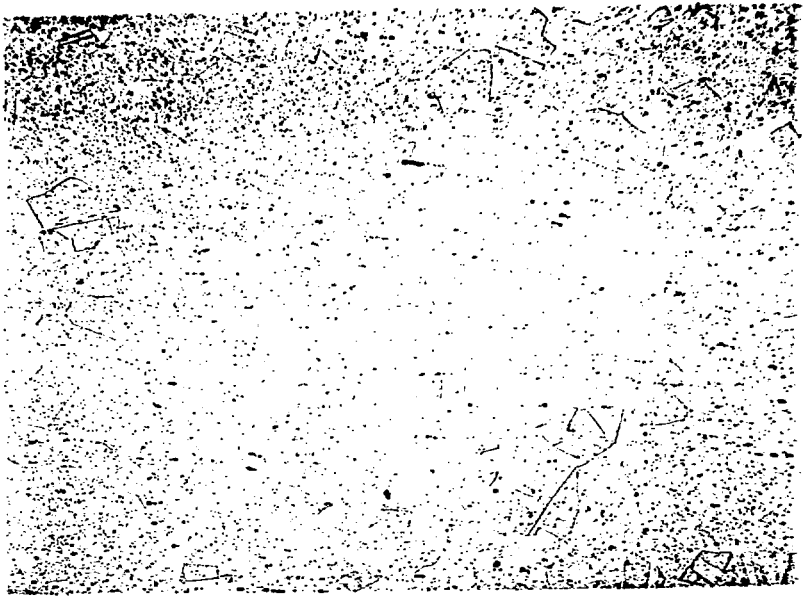

Fig. 9a 100 µm 200X

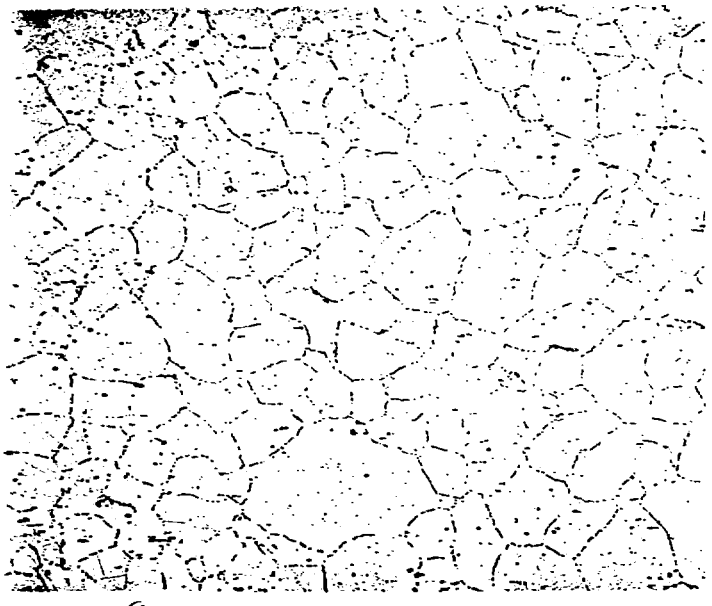

9d 100 µm 200X

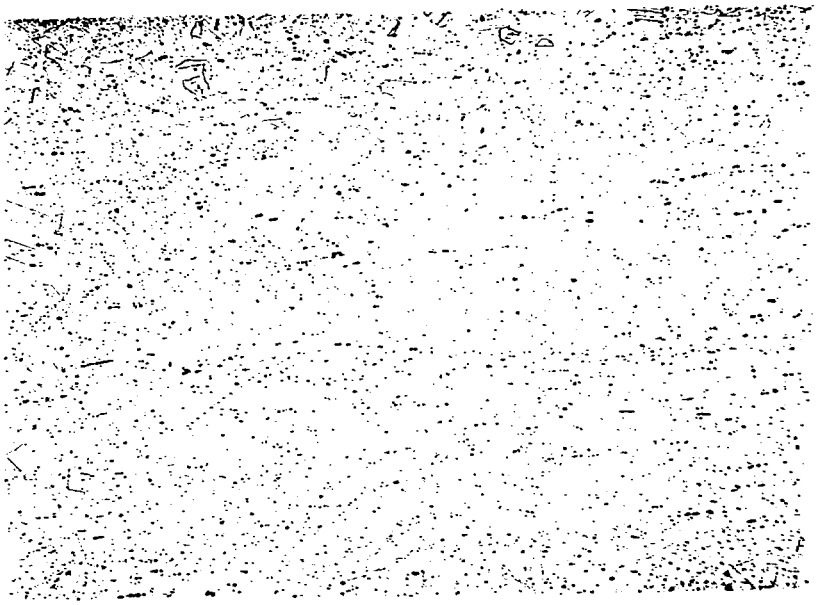

Fig. 9c 100 µm 200X

Fig. 9e 100 µm 200X

9f 100 µm 200X

10b.

K 14882

Fig 10a.

0.5μm

K 14872

10c

K 14891 YE-13304

10d.

K 14901

10f

k 14922

YE-13801

YE-13801

10e

k 14912

YE-13802


ORNL PHOTO 4021-88
BASE ALLOY - Fe - 12Cr - 20Mn - 0.25C, 20%CW + AGED 168h AT 800°C
BASE ALLOY, PARTIAL RECRYSTALLIZATION + RECOVERY
COARSE $M_{23}C_6$
BASE ALLOY + Ti, RECRYSTALLIZATION
COARSE $M_{23}C_6$ + TiC
BASE ALLOY + Ti, V, B, P SLIGHT RECRYSTALLIZATION
COARSE $M_{23}C_6$, FINE MC
BASE ALLOY + W, Ti, V, B, P PARTIAL RECRYSTALLIZATION
COARSE $M_{23}C_6$ + σ, FINE MC
1 μm (12,500X)

Fig. 11

Fig. 12a YE-13778 0.1μm

12a.

12c

12e

12f.

YE 13386

K 14956

ORNL-DWG 88-6594AR

DECAY OF INDUCED RADIOACTIVITY FOR FUSION REACTOR FIRST WALL

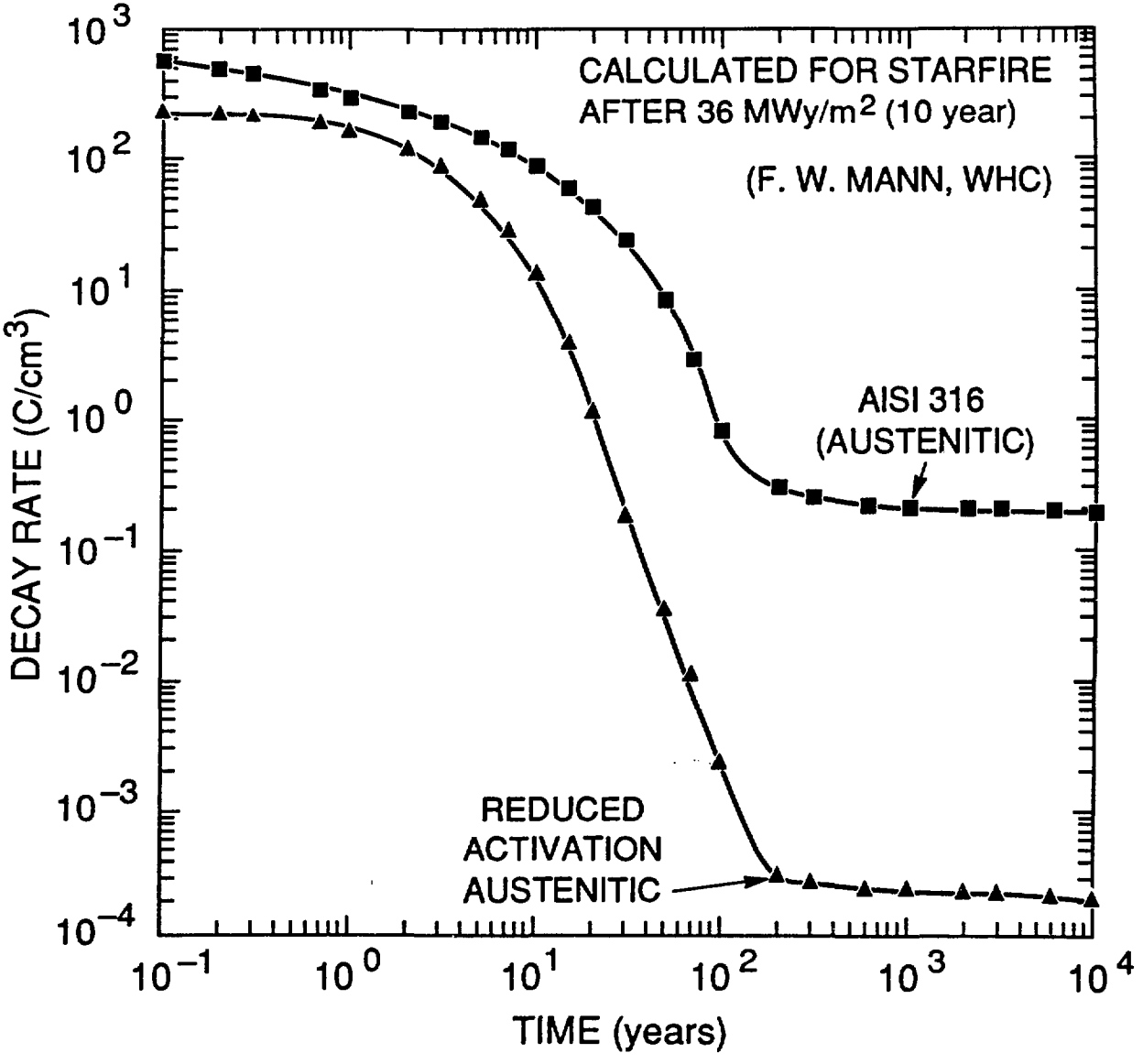

Fig. 13

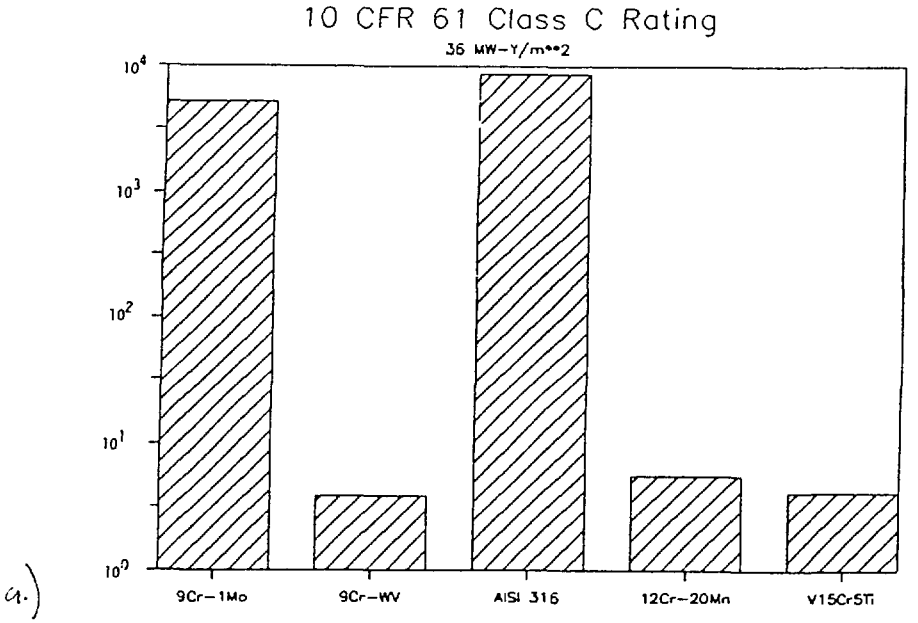
10 CFR 61 Class C Rating
36 MW-Y/m**2
10^4
10^3
10^2
10^1
10^0
9Cr-1Mo
9Cr-WV
AISI 316
12Cr-20Mn
V15Cr5Ti

a.)

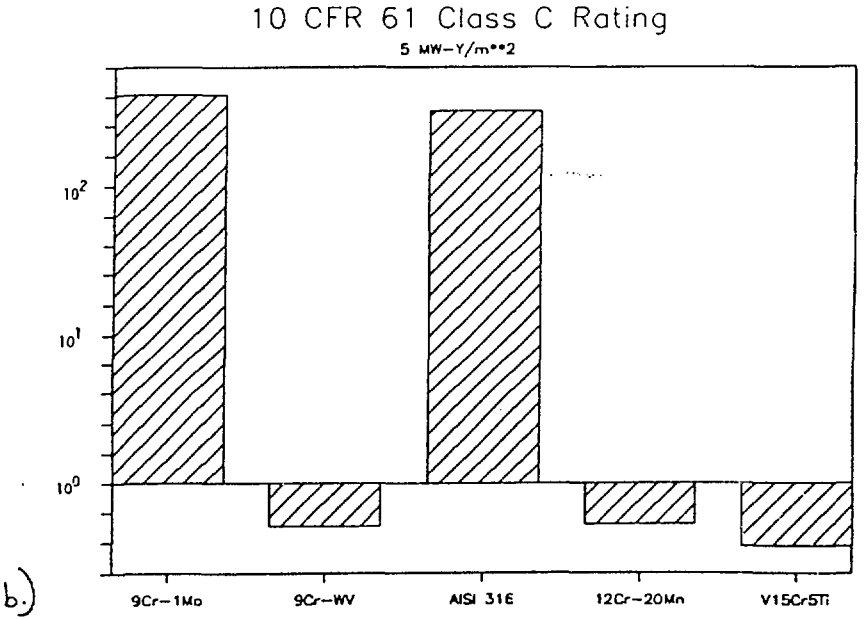
10 CFR 61 Class C Rating
5 MW-Y/m**2
10^2
10^1
10^0
9Cr-1Mo
9Cr-WV
AISI 316
12Cr-20Mn
V15Cr5Ti

b.)

Fig. 14.